Benchmarking EUV mask inspection beyond 0.25 NA

Kenneth A. Goldberg[1], Iacopo Mochi[1], Patrick P. Naulleau[1], Hakseung Han[2], Sungmin Huh[3]

[1]Center for X-Ray Optics, Lawrence Berkeley National Laboratory, Berkeley, CA 94720, USA
[2]Photomask Team, Samsung electronics, Ban-Wol, Hwasung, Kyunggi, Korea 445-701
[3]SEMATECH, 255 Fuller Road, Suite 309, Albany, NY 12203, USA

ABSTRACT

The SEMATECH Berkeley Actinic Inspection Tool (AIT) is an EUV zoneplate microscope dedicated to photomask research. Recent upgrades have given the AIT imaging system selectable numerical aperture values of 0.25, 0.30, and 0.35 (4× equivalent). The highest of which provides resolution beyond the current generation of EUV lithography research tools, giving above 75% contrast for dense-line features with 100-nm half-pitch on the mask, and above 70% for 88-nm half-pitch. To improve the imaging system alignment, we used through-focus images of small contacts to extract aberration magnitudes and compare with modeling. The astigmatism magnitude reached a low value of 0.08 waves RMS. We present the results of performance benchmarking and repeatability tests including contrast, and line width measurements.

Keywords: extreme ultraviolet lithography, EUV, mask inspection, zoneplate, actinic inspection, linewidth, contrast.

1. INTRODUCTION

Patterned-mask inspection is a critical step in the development of any lithography technology. This is especially true for EUV lithography where relevant defect sizes can be on the order of 20–50-nm wide or 1–2 nm tall[1], and the masks' optical properties are highly wavelength specific. In EUV lithography, the mask surface is a complex optical system with nanometer scale features. Below the patterned absorber and protective buffer layers, a multilayer coating on a smooth, low-thermal-expansion glass substrate provides a resonant reflection for EUV light.

The mask surface structure is highly sensitive to contamination from particles above, within, or below the multilayer, and from carbon deposition in the presence of EUV light's ionizing radiation. It may also be sensitive to thermal damage, oxidation, and damage caused by various inspection methods.

The acute sensitivity to the wavelength-dependent material properties and resonant-reflective multilayer mirror structure makes inspection with EUV light a necessary step in the technology development process. Whether EUV "actinic" inspection will be required in production is a subject of open debate and active research; yet in this pre-commercial period, it is clear that the early availability of high-quality aerial image measurements from patterned masks is providing detailed feedback for reticle development, defect sensitivity evaluation, aerial image modeling, and answers to other important questions. Aerial image inspection is complementary to lithographic printing; it provides continuous image intensity data without the constraints of photo-resist printing.

The SEMATECH Berkeley Actinic Inspection Tool (AIT) is a synchrotron-based EUV microscope that produces high quality aerial image measurements of mask surfaces[2,3]. The AIT has been used to study the detectability and printability of EUV mask blank defects[4], and in the determination of the critical sizes of EUV mask substrate defects[5], and to validate defect-repear techniques[6], among other research.

Hardware upgrades performed in 2008 have given the AIT new capabilities and improved imaging performance. Additional work to assess and correct the optical aberrations through improved alignment have yielded much lower astigmatism than before. These upgrades and improvements, and the results of several benchmarking tests, are the subject of this paper. Following a description of the optical imaging system configuration and a discussion of the recent upgrades, we preset a brief analysis of low-ordered aberrations in the AIT and measurements recorded during system alignment. We have measured the imaging contrast of dense-line features as small as 88-nm on the mask and we will present the results of line width measurement repeatability studies.

2. SYSTEM DESIGN AND UPGRADES

The AIT system, which has been described previously[2], has been upgraded in several ways: new zoneplates for higher imaging resolution were installed, the alignment was improved to reduce aberration magnitudes, and an angle-scanning mirrors for improved illumination uniformity has been upgraded for speed and repeatability[3].

The AIT operates on a bending magnet beamline at the Advanced Light Source, Lawrence Berkeley National Laboratory. The beamline source has a monochromator that provides stable, EUV illumination with a tunable wavelength centered at 13.4 nm. To avoid chromatic aberration from the zoneplate (primarily focus blur), we operate the monochromator with narrow band illumination with $\lambda/\Delta\lambda$ of approximately 1450.

The beamline optics include a Kirkpatrick-Baez (KB) mirror pair, and a 20× Schwarzschild objective to demagnify the source and increase the illumination solid angle. To expand the illumination area, the mask is positioned 200–400 μm below the Schwarzschild objective's focal plane. With a static-mirror configuration, the mask illumination has visible non-uniformities that likely arise from imperfections and carbon contamination in the upstream mirrors. We create more uniform illumination by oscillating the angle of the horizontal KB mirror during exposures[3]—a dedicated oscillating scanning motor was added to the mirror stage in 2008. The angle scanning sweeps the illuminated area back-and-forth in the *x*-direction with a scanning frequency of approximately 1–2 Hz, depending on the amplitude.

Measurements of contrast through-focus have shown that the native illumination coherence of the beamline is very high. The angle scanning illumination increases the partial coherence σ value to between 0.1 and 0.2, depending on the NA value and scan-angle amplitude[3].

The configuration of the AIT's imaging optics and light path is shown schematically in Fig. 1 and described in Table 1. Before 2008, only one zoneplate was available for imaging. Now, the zoneplate design has been modified to include an array of five, user-selectable zoneplates with different optical properties: magnification values are 680, 907, and 1000×; numerical aperture (NA) values are 0.0625, 0.075, and 0.0875. These NA values emulate the resolution of a 4× EUV stepper with NA values of 0.25, 0.30, and 0.35. The zoneplates are defined in a patterned nickel layer in a silicon-nitride membrane. The 6°-incident beam passes through an open region of the absorber and illuminates a mask area approximately 30-μm-wide. Each zoneplates has a circular pupil, with an off-axis design that **provides** the angular separation of the various diffraction orders. The first-order focused image is formed with high magnification directly on a back-thinned, back-illuminated CCD camera; the zoneplate's undiffracted zeroth-order light is steered below the CCD sensor.

Table 1. AIT imaging parameters.

property	Value
wavelength	13.4 ± 0.01 nm, tunable
available NA values	{0.25, 0.30, 0.35} (4×) {0.0625, 0.075, 0.0875}
zoneplate focal length(s)	680, 750, 1000 μm
magnification	680, 907, 1000×
exposure time	0.5 s, alignment 25–35 s, high resolution
CCD pixel size, number	13.5 μm, 2048 × 2048
pixel equivalent mask size	19.8, 14.9, 13.5 nm
observable mask area	approx. 31 μm for 907×
high-quality field of view	approx. 2–8 μm, dependent on feature size.
typical data collection rate	approx. 250 images / 8h
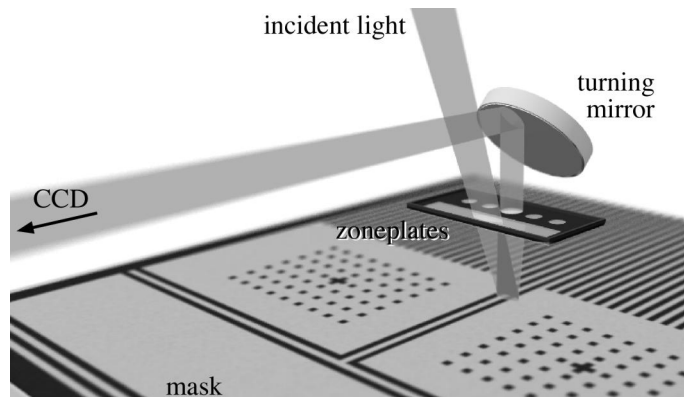
Fig. 1. AIT imaging optics and light path, not to scale. A zoneplate array, held 0.68 to 1.0 mm above the mask surface, projects a high-magnification image of the illuminated mask surface onto a CCD camera, after reflection form a 45° multilayer-coated turning mirror.

To ensure that the central ray falls close to the vertical center of the CCD camera, an additional *tilt* degree of freedom was added to the turning-mirror mount. The tilt stage is controlled by a *New Focus Picomotor* and provides ±1° of adjustment *in situ*.

Two recent upgrades have doubled the linear pixel density for the image collection, resulting in improved contrast for small feature sizes. Three different zoneplates were installed with a 750-µm focal length (previous was 1000 µm) raising the magnification ratio from 680× to 907×. In addition, the previous CCD camera was replaced with a newer model that has smaller, 13.5-µm square, pixels (previous was 20 µm). Now each CCD pixel corresponds to approximately 15 nm on the mask, whereas the previous value was approximately 30 nm.

3. ABERRATION MEASUREMENTS

In recording the projected aerial images, the wavefront quality of the objective lens affects nearly every performance metric. The image blur caused by aberrations reduces the resolution, the image peak intensity and contrast of small lines, the local image slope at feature edges, and the quality of linewidth measurements.

The AIT has a single zoneplate lens as the only image-forming element; the lens is designed to be aberration-free at one single point in the mask. Owing to the zoneplate's geometry, small diameter, and off-axis design, field dependent aberrations increase in all directions away from the central point and limit the field of view to a few microns diameter. However the observable mask area recorded by the AIT is much larger, typically about 32-µm wide.

Owing to the complexity and interdependence of the alignment degrees of freedom, the subtle influence of the aberrations on the image quality, and the feedback limitations that naturally occur for an EUV optical system, fine alignment of the AIT is not a trivial exercise. Given the aberration field-dependence, we assume that the primary origin of aberrations in the AIT is misalignment. By understanding the expected aberration behavior, and quantifying observed aberration magnitudes across the viewable area, we have been able to significantly improve the AIT alignment and with it the imaging quality.

To quantify aberration behavior across the field of view, we developed an optical model of the AIT using *ZEMAX*®. The predicted behavior of the low-spatial-frequency aberrations across a 30-µm-wide mask area is shown in Fig. 2.
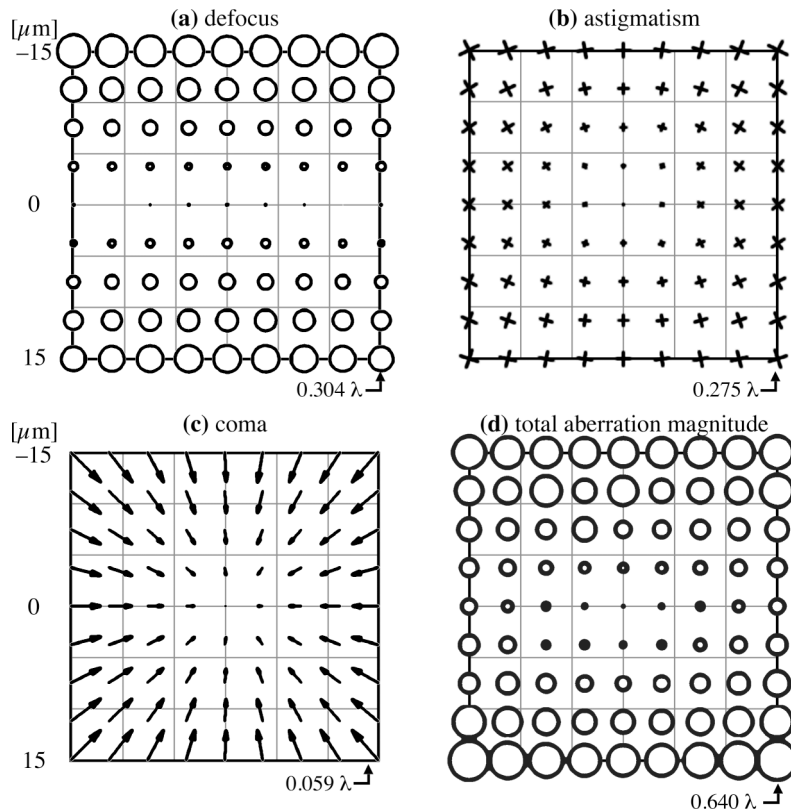

Fig. 2. Modeling the field-dependent aberrations of the AIT in its ideal alignment configuration. Here, representations of low-spatial-frequency aberrations across a 30-µm wide square area are shown. The modeled zoneplate is a 0.0875-NA lens (0.35-NA 4× equivalent) with a 750-µm focal length. In each case, the scale is shown in the lower-right corner, and the aberration magnitudes are represented by the linear symbol size. **(a)** The focal plane is tilted at 6°. **(b)** The astigmatism orientation is represented by the rotation of the crosses. **(c)** The coma orientation is represented by the arrows. **(d)** The total aberration magnitude, including defocus, is zero at the center of the field, and increases in all directions.

Figure 3 shows two through-focus image series extracted from an array of 175-nm (mask) square contacts using different zoneplates, and different alignment states of the AIT. The 90° rotation of the elliptical shape on either side of best focus clearly indicates the presence of astigmatism in both cases. We estimate the orientation and magnitude of the astigmatism by comparing the observed ellipticity to through-focus image simulations using a two-dimensional Gaussian fit.

Both image series shown in Fig. 3 were extracted from the points in the observable field with the lowest aberration magnitude. For the April 2008 series, the calculated RMS astigmatism error magnitude was 0.23 waves (i.e. λ/4.35 or 3.1 nm). We believe that this relatively large aberration magnitude may be attributable to a physical tilt of the zoneplate in its mount.

Following zoneplate replacement and re-alignment, the RMS astigmatism error magnitude was reduced to 0.08 waves (i.e. λ/12.5 or 1.1 nm). During the alignment, we measured the astigmatism across the viewable mask area, and used the *ZEMAX*® model to guide our alignment toward the center of the field. The wavefront error may be further reduced by continued alignment efforts.

April 2008: RMS astigmatism error magnitude is 0.23 waves (i.e. λ/4.35 or 3.1 nm).
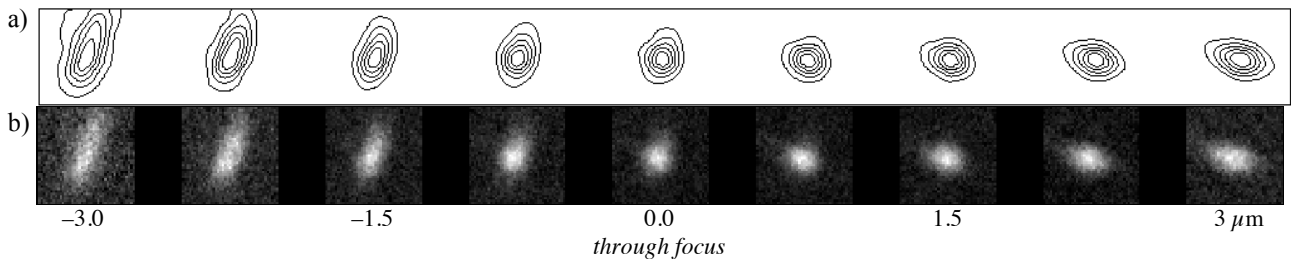
August 2008: RMS astigmatism error magnitude is 0.08 waves (i.e. λ/12.5 or 1.1 nm).
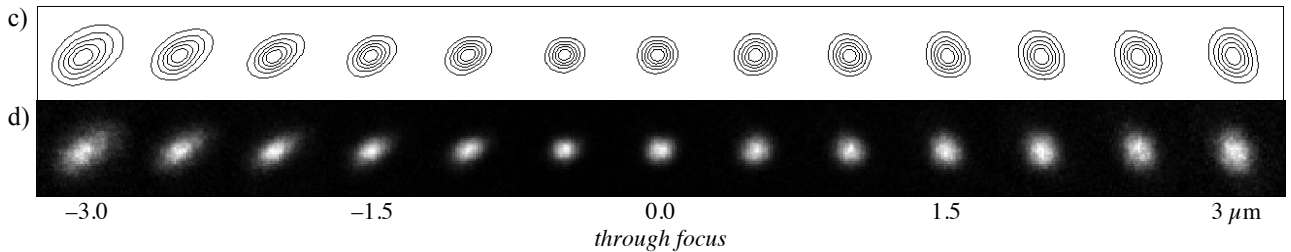
Fig. 3. Through-focus series showing the appearance of a 175-nm (mask) square contacts in two different zoneplates and different alignment states of the AIT, at 0.0875-NA (0.35-NA 4× equivalent). Individually-scale intensity images are shown in **(b)** and **(d)**. Spatially-filtered contour plots shown in **(a)** and **(c)** reveal the shape changes that are used for aberration fitting. The square images are 627-nm wide.

4. CONTRAST TRANSFER FUNCTION—CTF

The CTF of an optical system is the ratio of the contrast in the image to that in the object as a function of the feature size. The more familiar modulation transfer function (MTF) is strictly defined for incoherent illumination conditions ($\sigma = \infty$). The CTF of a high-quality imaging system is a function of its illumination coherence properties, the pupil's shape and numerical aperture, and the incident light wavelength. Coherently illuminated systems are expected to maintain high contrast, with a sharp drop near the resolution limit. Partially coherent optical systems typically have a range of illumination angles that causes the contrast to roll off more gradually for smaller feature sizes. Aberrations can reduce the contrast, and hence the CTF: their contributions may vary with both the direction and size of features being imaged.

We have previously reported CTF measurements using a 0.0625-NA (0.25-NA 4× equivalent) zoneplate lens[2]. Similar measurements using dark-field elbow patterns on an *Intel* mask were performed using the new 0.0875-NA (0.35-NA 4× equivalent) lens, and the comparison showed improved contrast below 250-nm linewidth[3]: The open-circle plot in Fig. 4 contains the contrast versus linewidth data. These elbow pattern measurements were performed in April 2008, with the AIT alignment state described above. While the presence of astigmatism can degrade image contrast, some line orienta-

tions can maintain high peak contrast through-focus. The elbow patterns studied here contain two pairs of nested elbow sets with parallel-line orientations corresponding to (0°, 45°, 90°, and 135°). The elbow contrast data shown in Fig. 4 represents the highest measured contrast of the four available elbow directions. The smallest elbow feature size available was 100-nm linewidth.

Following the August 2008 zoneplate replacement and re-alignment, a new CTF measurement was performed. A *Samsung* mask containing programmed-defect arrays and feature sizes as small as 88 nm was created specifically for these measurements. The basic pattern consists of 30 parallel, dense lines with pattern defects spaced widely enough that the regions between them can be used for contrast analysis through-focus. Patterns representing several different linewidths were measured repeatedly to ascertain the measurement repeatability. The average and standard deviation data from the contrast measurement repeatability tests is shown as filled circles in Fig. 4. Additional information about the image analysis methods is given in Section 6. The individual contrast measurements used to for the average and standard deviations are shown in Fig. 6 with the linewidth measurements.

Using the 0.0875-NA zoneplate objective the AIT maintains above 70% contrast in 88-nm dense line features, the smallest mask features examined to date. The 88-nm mask feature size corresponds to a printed size of 22 nm in a 4× system, and 18 nm in a 5× system. Further improvements in the CTF may come from continued progress in reducing the aberration magnitude through alignment.

Scattered background light is a separate issue that complicates contrast analysis in the AIT. We frequently observe a non-uniform, diffuse background light pattern that varies depending on the pattern size and direction in the illuminated region of the mask. Since the scattered light appears to be weakest with isolated dark-field patterns, we conclude that the light comes from the illuminated mask pattern. One explanation may be an overlapping zoneplate zeroth-order (undiffracted) light path generated by diffraction from mask patterns that may be at the edge or outside of the observable region of the mask, primarily in the off-axis direction. We compensate for this background signal by mathematically subtracting the light intensity that we measure in dark areas of the mask adjacent to the features we are measuring.
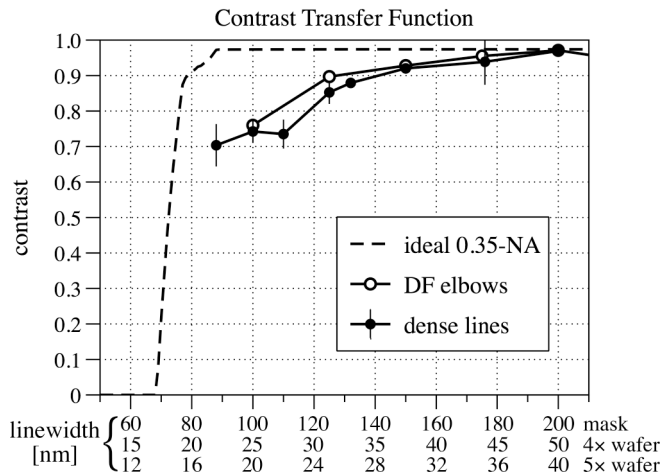
Fig. 4. The CTF of 0.0875-NA (0.35-NA 4× equivalent) zoneplate lenses was measured using two different image patterns: dark-field elbows, and dense lines. The dashed line shows the ideal performance for an aberration-free optical system with a partial coherence σ value of 0.1, close to the measured value[3]. Dense-line mask features with 88-nm linewidth are the smallest we have measured to date. Equivalent wafer-printed sizes for 4× and 5× systems are also given.

5. LINEWIDTH MEASUREMENTS

Simultaneous with the CTF measurements, linewidth (i.e. *critical dimension*, or CD) measurement studies were made using the dense line patterns described above. The AIT was in the alignment state described in Section 3 for August 2008. Our goal was to test the repeatability of the measurements, to better understand measurement uncertainties. The goal of the linewidth measurements was to quantify the variation in measured linewidths when a consistent normalized intensity threshold value is used. For each dense-line pitch, global threshold values were based on the average of the thresholds that produce 1:1 line spacing within each independent measurement series.

For each feature size, we identified a region of the dense line pattern and examined its behavior through-focus in up to ten independently measured data series. Because the depth of focus is feature-pitch dependent, we varied the longitudinal

(*focus*) step size from 0.4 to 0.8 μm, for the different feature sizes. Ten sub-regions measuring 4 CD × 8 CD (with the long dimension parallel to the line orientation) were extracted and studied separately through focus. In each sub-region, the best-focus image was identified by finding the peak contrast value within the series; linewidth measurements were only made on the best-focus sub-images.

Aerial image linewidth measurements require the definition of a consistent intensity threshold value for each feature size. Within the sub-image through-focus series, we calculated the threshold value that produces 1:1 line-to-space ratio at best-focus, and then averaged those threshold values to define a single global threshold for each given feature size. Before calculation, linear intensity variations were corrected in each sub-image using the method described in Section 6.

Typical best-focus images for four different dense-line pattern sizes are shown in Fig. 5. The figure shows normalized aerial images, binarized images using a threshold value that gives 1:1 line-to-space ratio, and intensity cross-section line-outs calculated by averaging the pattern in the vertical direction.
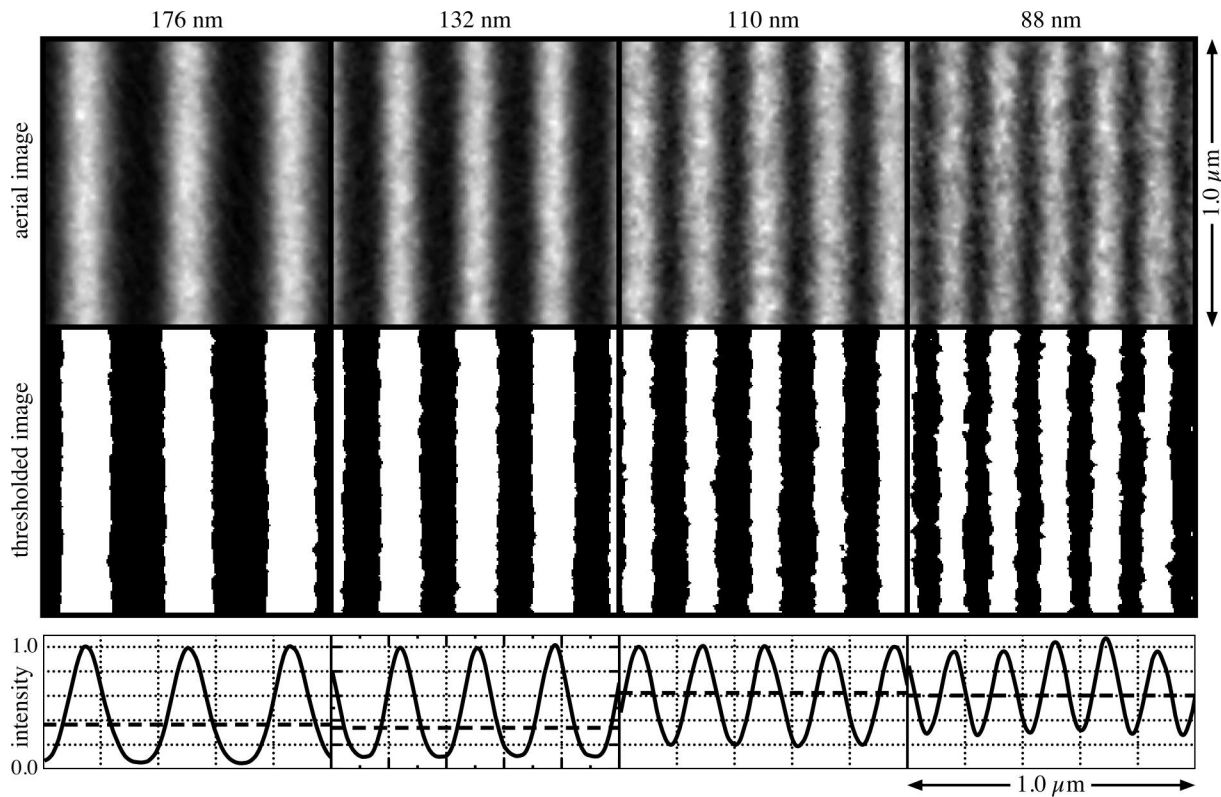
Fig. 5. Analysis of dense-line patterns with four different linewidth values, as shown. Shown are normalized aerial images from a 1-μm square region, a binarized version of the same, using a threshold value that gives 1:1 line-to-space ratio, and intensity cross-section line-outs calculated by averaging the pattern in the vertical direction. Binarized images such as these are collected at best-focus, and linewidths are calculating using a global-average threshold value for each feature size.

Figure 6 shows the individual mask CD and contrast measurements for multiple independent series and four different pattern feature sizes.
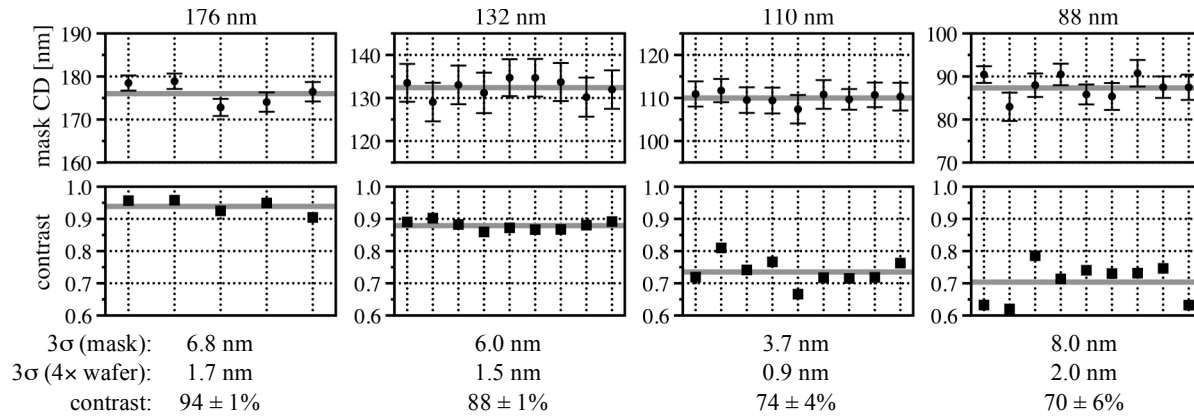
Fig. 6. Linewidth (CD) and contrast repeatability measurements are shown for four different dense-line pattern sizes. Each data point represents the average linewidth and standard deviation at best focus, from measurements in ten regions of independent through-focus series. The peak contrast was simultaneously evaluated at 10 different image positions: the error bars form each point are smaller than the black squares.

6. NOTES ON CONTRAST AND LINEWIDTH MEASUREMENTS

Great care was taken to extract the highest measurement quality from the aerial image data. In particular, compensating even a few percent intensity non-uniformity within the sub-images, or from one sub-image to the next, can reduce the linewidth uncertainty and improve the contrast measurement.

6.1 Sub-image normalization. The image sub-regions subjected to detailed analysis were typically 4 CD wide (2 complete lines) by 6 to 8 CD parallel to the direction of the lines. To detect and compensate for slowly-varying intensity changes, we calculated the total intensity level in each row, perpendicular to the line direction, and normalized the sub-region intensity using a linear fit to that data. To compensate for uniform changes in intensity from one region to the next, we scaled each sub-image's intensity to match a constant total intensity level.

6.2 Contrast measurement. Aerial-image contrast is defined as

$$contrast \equiv \frac{max - min}{max + min}. \tag{1}$$

Measuring contrast accurately requires that care be taken to reduce sensitivity to spurious extreme values. We based our sub-image contrast measurements on the average line-intensity profiles, calculated parallel to the line direction. Such intensity profiles are shown in Fig. 5. We found that the sub-image normalization described in Section 6.1 was an important preliminary step for reducing measurement uncertainty.

6.3 Linewidth measurement. Following image normalization, linewidth measurements were based on calculated normalized intensity threshold values that produce 1:1 line spacing. Concentrating on the dark-line width, we average the linewidths in each row of the sub-image to produce a single measurement. As described in Section 5, linewidth repeatability tests conducted with many through-focus series sought to quantify the uncertainty of a single series.

7. CONCLUSION

The aerial image measurement capabilities of the AIT have been expanded to include multiple, user-selectable lenses, with numerical aperture values up to 0.0875 (matching a 0.35-NA 4× projection tool). The magnification and CCD camera resolution have been increased to produce higher image contrast: above 70% at 88-nm half-pitch. Through system modeling and aberration measurements, based on through-focus measurements of contact arrays, we have reduced the astigmatism magnitude to 0.08 waves RMS.

With improved imaging performance, we have investigated the linewidth and contrast measurement capabilities of the AIT through a series of repeatability tests performed with multiple linewidths, from 200 nm down to 88-nm. Linewidth

repeatability measurements produce 3σ values between 3.7 and 8.0 nm (between 0.9 and 2.0 nm, in 4× wafer scale). From independent through-focus series, contrast measurement standard deviations can be as low as 1% for larger features sizes, but increase below 132 nm half-pitch.

For the AIT, the primary challenges for high-quality recording and analysis of EUV aerial images are illumination non-uniformities, signal-to-noise limitations from insufficient exposure times, fine-alignment to minimize aberrations, and the coupling of field-dependent aberrations with lateral mask motion during through-focus series. Detailed measurements such as these have helped to quantify these effects, and will lead to improved measurements and methods in the near future. Aberrations are modeled, measured, and minimized through system alignment; illumination non-uniformities can be detected and compensated in periodic patterns; and improved hardware can resolve mask motion during measurement series.

Research tools such as the AIT provide a vital service in the development of EUV lithography by providing early research and detailed feedback for mask development. By prototyping and benchmarking aerial image measurement techniques, research conducted with the AIT can directly benefit the commercial development of EUV mask inspection tools, which are urgently needed.

ACKNOWLEDGMENTS

REFERENCES

1. W. Cho, H.-S. Han, K. A. Goldberg, P. A. Kearney, C.-U. Jeon, "Detectability and printability of EUVL-mask blank defects for the 32-nm HP node," *Proc. SPIE* **6730**, 673013-1-9 (2007).
2. K. A. Goldberg, P. P. Naulleau, A. Barty, S. B. Rekawa, C. D. Kemp, R. F. Gunion, F. Salmassi, E. M. Gullikson, E. H. Anderson, H.-S. Han, "Performance of actinic EUVL mask imaging using a zoneplate microscope ," *Proc. SPIE* **6730**, 67305E-1-12 (2007).
3. K. A. Goldberg , P. Naulleau, I. Mochi, E. H. Anderson, S. B. Rekawa, C. D. Kemp, R. F. Gunion, H.-S. Han, S. Huh, "Actinic EUV Mask Inspection beyond 0.25 NA," *J. Vac. Sci. & Technol. B*, (2008) *in press*.
4. W. Cho, H.-S. Han, K. A. Goldberg, P. A. Kearney, C.-U. Jeon , "Detectability and printability of EUVL-mask blank defects for the 32-nm HP node ," *Proc. SPIE* **6730**, 673013-1-9 (2007).
5. H.-S. Han, W. Cho, K. A. Goldberg, E. M. Gullikson, C.-U. Jeon, S. Wurm, "Determining the critical size of EUV-mask substrate defects," *Proc. SPIE* **6921**, 62911Y (2008).
6. S.-Y. Lee, G.-B. Kim, H.-S. Sim, S.-H. Lee, *et al.*, "Analysis of process margin in EUV mask repair with nanomachining," *Proc. SPIE* **7122**, *in press*.